Environmental Technology & Innovation 40 (2025) 104504

Contents lists available at ScienceDirect

Environmental Technology & Innovation

journal homepage: www.elsevier.com/locate/eti

Nano-magnetite enhanced biomass tolerance towards inhibition in the degradation of phenol and p-cresol in anaerobic membrane bioreactor

Rifki Wahyu Kurnianto [a,b,*], Mostafa Elshourbagy [a], Eman Rageh [a], Beatriz Egerland Bueno [a,c], Daniel Cerqueda-García [d,e], Julian D. Muñoz Sierra [a,f], Henri Spanjers [a], Jules B. van Lier [a]

[a] Section Sanitary Engineering, Department of Water Management, Delft University of Technology, Stevinweg 1, Delft 2628 CN, the Netherlands
[b] Department of Chemical Engineering, Universitas Gadjah Mada, Jalan Grafika No. 2, Sleman 55281, Indonesia
[c] Laboratory of Environmental Biotechnology, Department of Food Engineering, University of Sao Paulo, 225, Duque de Caxias Norte, Pirassununga, Sao Paulo 13635-900, Brazil
[d] Institute of Ecology, National Autonomous University of Mexico, Circuito ext. Sn, Cd. Universitaria, Mexico City, Mexico
[e] Red de Manejo Biorracional de Plagas y Vectores, Instituto de Ecología, A. C. – INECOL, Xalapa 91073, Mexico
[f] KWR Water Research Institute, Groningenhaven 7, Nieuwegein 3433 PE, the Netherlands

ARTICLE INFO

Keywords:
Phenolics
Magnetite
Nanoparticles
AnMBR
Biodegradation

ABSTRACT

The anaerobic degradation of phenolic compounds presents substantial challenges due to their toxicity to methanogenic biomass and inherently low conversion rates. Recent studies indicate that nano-magnetite can stimulate direct interspecies electron transfer (DIET), potentially enhancing phenol conversion and methane production. This study employed two anaerobic membrane bioreactors (AnMBRs) to investigate phenol and p-cresol degradation under stepwise increasing loading rates, with complete retention of biomass in both reactors. While AnMBR-C served as a control, nano-magnetite was additionally supplemented to reactor AnMBR-M at a concentration of 40 mmol/L in Phase 1 and 20 mmol/L in Phase 2. Results demonstrated that AnMBR-M supplemented with 20 mmol/L nano-magnetite tolerated higher phenolic loading rates compared to AnMBR-C. In Phase 2, a higher total Fe concentration was observed in AnMBR-M, suggesting an enhanced electron transfer mechanism via dissimilatory iron reduction-oxidation cycle. Follow-up batch experiments revealed that magnetite-adapted biomass had more tolerance to phenol inhibition. A 16S-rRNA sequencing was conducted to characterize microbial communities within both reactors. Results suggested that DIET was stimulated in Phase 1, as shown by the enrichment of the electrogenic *Pseudomonas* and *Methanolinea* in AnMBR-M. However, the possibly stimulated DIET in Phase 1 could not alleviate the inhibition caused by excessive 40 mmol/L nano-magnetite dosage. Notably, there was no significant difference between the genera of AnMBR-C and AnMBR-M by the end of Phase 2. However, short-chain fatty acid degrader *Mesotoga* was more enriched in AnMBR-M. Moreover, species-level analysis showed that AnMBR-M had a sixfold higher relative abundance of *Methanosaeta harundinacea* compared to AnMBR-C.

* Corresponding author at: Section Sanitary Engineering, Department of Water Management, Delft University of Technology, Stevinweg 1, Delft 2628 CN, the Netherlands.
E-mail addresses: r.w.kurnianto@tudelft.nl, rifki.wahyu.k@ugm.ac.id (R.W. Kurnianto).

https://doi.org/10.1016/j.eti.2025.104504
Received 12 June 2025; Received in revised form 26 August 2025; Accepted 6 September 2025
Available online 8 September 2025

1. Introduction

Phenolic compounds are major pollutants that can be commonly found in petrochemical wastewaters such as coal gasification wastewater and bitumen fume condensate (García Rea et al., 2023; Muñoz Sierra et al., 2020). Releasing these substances without proper treatment has adverse impacts on the environment (Jung et al., 2022). In choosing treatment systems for addressing these compounds, anaerobic digestion is regarded as the preferred biological wastewater treatment for its negligible energy demand and the recovery of the pollutants' biochemical energy in the form of biogas (Castellano-Hinojosa et al., 2018). Multiple studies reported a high dependency of anaerobic phenol degradation on the syntrophic associations between the phenol-degrading bacteria and the methanogens (Mostafa et al., 2020; Qiu et al., 2008). However, anaerobic degradation of aromatic compounds is considered challenging, due to their refractory and inhibitory properties to the methanogens (Garcia Rea et al., 2022; Li et al., 2018).

Recent studies reported an electron transfer pathway between syntrophic-methanogenic communities, making use of direct interspecies electron transfer (DIET) (Xu et al., 2019). In the DIET pathway, electrons are transferred without utilizing molecular H_2 as an electron carrier between acidogenic or acetogenic bacteria and methanogens that reduce CO_2 to CH_4. This DIET mechanism distinctly mitigates the thermodynamic constraints in the anaerobic degradation of phenol by reducing its dependency on the transfer of H_2 molecules (Wang et al., 2021). Furthermore, studies also showed that DIET-stimulated microbial communities have higher tolerance toward inhibitory compounds like ammonia, especially in reactors with conductive material addition (Gahlot et al., 2020).

Nano-magnetite is one of the conductive materials that have been reported to stimulate DIET in the anaerobic degradation of phenolic compounds. For example, Yan et al. (2018) reported that nano-magnetite supplementation increased low molecular weight

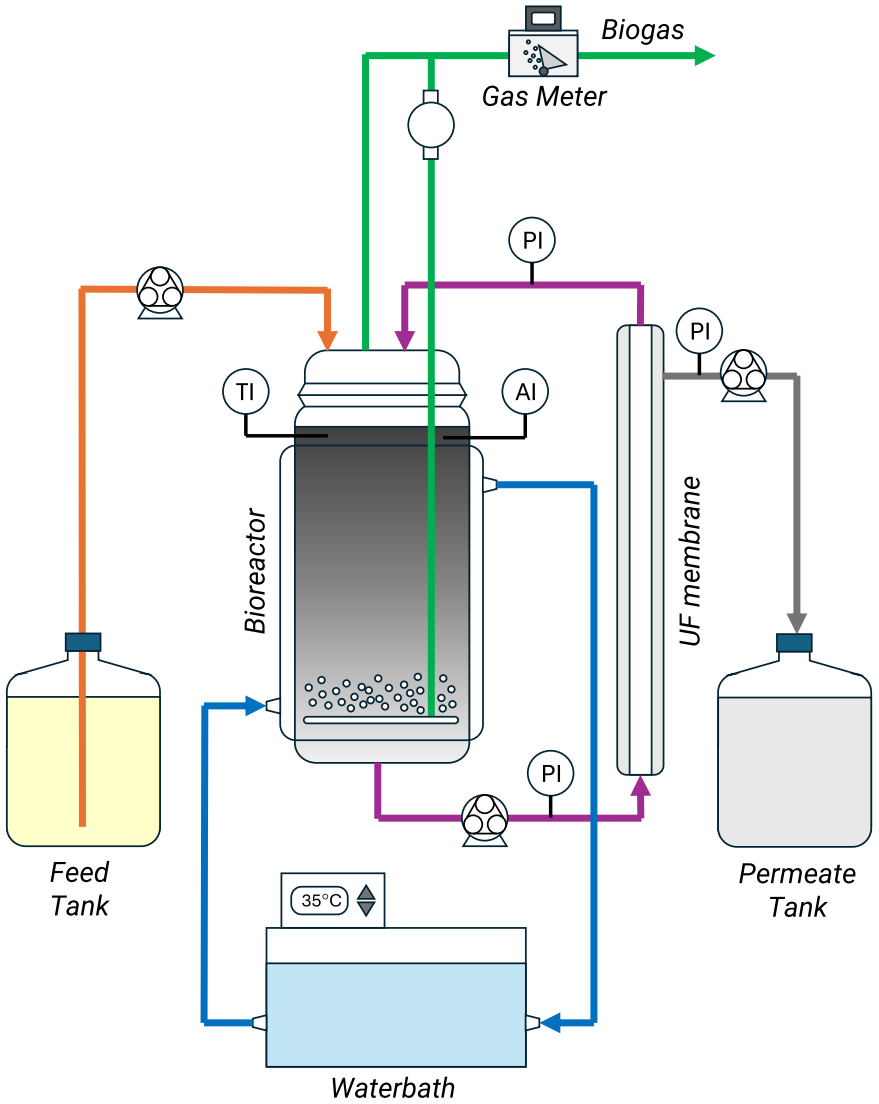

Fig. 1. Schematic representation of the AnMBR setup for the AnMBR experiment.

extracellular polymeric substances (EPS) in anaerobic batch reactors, altered microbial communities, and improved extracellular electron transfer, leading to enhanced phenol conversion and methane production rates. Moreover, He et al. (2019) showed that magnetite supplementation enhanced the phenol degradation rate by 20.1 %, but failed to enhance the benzoate degradation rate. Additionally, Jung et al. (2022) revealed that magnetite supplementation significantly enhanced the phenol degradation by 9.0 – 68.0 % in terms of methane production rate and reduced the lag time by 7.9 – 48.0 %.

However, studies related to the application of nano-magnetite were mostly conducted in batch-fed reactors. The application of nano-magnetite in continuous-flow reactors is constrained by the continuous wash-out of the small-sized nano-magnetite. Furthermore, the anaerobic degradation of phenolic compounds yields very low energy for microbial growth. Consequently, the potential wash-out of phenol degraders may impede the long-term effectiveness of conventional sludge bed reactors.

In the application of conductive materials to enhance phenol conversion in anaerobic high-rate reactors, the primary challenge is the effective retention of both nano-magnetite and (newly grown) microbial biomass. This challenge can be addressed by using an anaerobic membrane bioreactor (AnMBR), equipped with an ultrafiltration (UF) membrane for sludge separation, provided the membrane's nominal pore size is sufficiently small. In this study, the extent to which nano-magnetite enhances the performance of an AnMBR in terms of degradation rate of phenolic compounds, methane production rate, and maximum organic loading rate (OLR) were researched. To the authors' knowledge, this is the first study to investigate the role of nano-magnetite in the degradation of phenolic compounds in AnMBRs. Phenol and p-cresol were used as model compounds to simulate phenolic chemical wastewater, such as that from coal gasification wastewater and bitumen fume condensate (Garcia Rea et al., 2022; García Rea et al., 2023). Furthermore, microbial communities were analyzed to characterize the metagenome in the presence and absence of magnetite.

2. Materials and methods

2.1. Anaerobic membrane bioreactor (AnMBR) operation

Two AnMBRs with a 6.25 L liquid working volume were used. One reactor (AnMBR-M) was supplemented with nano-magnetite (Sigma Aldrich, USA), and the other one (AnMBR-C) served as the control reactor without the addition of nano-magnetite. Both reactors were equipped with a tubular ultrafiltration (UF) PVDF membrane with a nominal pore size of 30 nm, a length of 64 cm, and a diameter of 5.2 mm. The reactors were operated with an internal circulation rate of 1830 L/d, corresponding to a cross-flow velocity of 1.0 m/s. The temperature of the reactors was monitored with a temperature/pH sensor (Endress & Hauser, Memosens and Mettler Toledo) and was maintained at 35°C by recirculating heated water from a water bath (Tamson Instruments, The Netherlands) into the outer jacket layer. The same sensor was also used to monitor the pH of the mixed liquor. Fig. 1 illustrates the AnMBR setup used in this experiment.

Table 1
Feed composition in the AnMBR experiment. The column 'phenol and p-cresol concentration' shows the concentration of each phenolic compound in the feed (mg/L). The column 'Phenolic loading rate' shows the collective contribution to the organic loading rate by phenol and p-cresol. The nutrient composition was adopted from Garcia Rea et al. (2022).

Period	Stage	Phenol and p-cresol concentration (mg/L)	Acetate and butyrate concentration	Influent flow rate	Phenolic loading rate (g COD/(L.d))	Organic loading rate (g COD/(L·d)
Phase 1 (40 mmol/L Fe_3O_4)						
Day 0 – 16	1a	200	1 g COD/L each	1 L/d	0.16	0.48
Day 17 – 30	1b	300			0.24	0.56
Day 31 – 44	1c	400			0.31	6.34
Day 45 – 58	1d	600			0.47	0.79
Day 59 – 73	1e	900			0.71	1.03
Phase 2 (20 mmol/L Fe_3O_4)						
Day 0 – 3	2a	900	1 g COD/L each	0.4 L/d	0.28	0.41
Day 4 – 8	2b	900		0.6 L/d	0.42	0.62
Day 9 – 16	2c	900		0.8 L/d	0.56	0.82
Day 17 – 31	2d	900		1 L/d	0.71	1.03
Day 32 – 43	2e	1200			0.94	1.26
Day 44 – 62	2 f	1600			1.25	1.57
Day 63 – 73	2 g	2000			1.57	1.89
Day 74 – 87	2 h	2500			1.96	2.28
Day 88 – 94	2i	3000			2.34	2.67
Day 95 – 101	2j	3500			2.75	3.07
Day 102 – 126	2k	4000			3.14	3.46
Solution		**Composition**				
Micronutrients		$FeCl_3.6H_2O$ [2 g/L], $CoCl_2.6H_2O$ [2 g/L], $MnCl_2.4H_2O$ [0.5 g/L], $CuCl_2.2H_2O$ [0.03 g/L], $ZnCl_2$ [0.05 g/L], $NiCl_2.6H_2O$ [0.05 g/L], H_3BO_3 [0.5 g/L], $(NH_4)_6Mo_7O_{24}.4H_2O$ [0.09 g/L], Na_2SeO_3 [0.1 g/L], EDTA [1 g/L], Na_2WO_4 [0.08 g/L]				
Macronutrients		NH_4Cl [170 g/L], $CaCl_2.2H_2O$ [8 g/L], $MgSO_4.7H_2O$ [9 g/L],				
Buffer A		K_2HPO_4 [0.2 M]				
Buffer B		$NaH_2PO_4{\cdot}H_2O$ [0.2 M]				

Pressures at the influent, retentate, and permeate lines of the membrane module were measured by pressure sensors (AE Sensors, The Netherlands) ranging from −800–600 mbar to assess the transmembrane pressure (TMP). Similar sensors with a range of 0–200 mbar were used to monitor the head pressure of the reactor. Biogas flow rate was measured with a gas meter (Ritter, Germany) equipped with a clicker mechanism that registered a click for every 3.13 mL of gas passing through, and the methane content was measured utilizing gas chromatography as explained in Section 2.5.

The reactors were initially inoculated with biomass acquired from a full-scale UASB reactor treating petrochemical wastewater (Shell, Moerdijk, The Netherlands). Synthetic wastewater with medium salinity (~6 g Na^+/L) containing phenol and p-cresol with stepwise increasing concentrations, 1 g chemical oxygen demand (COD)/L of butyrate and 1 gCOD/L of acetate, 0.75 mL/g COD micronutrients, 1.5 mL/gCOD macronutrients, 2.2 mL/g COD phosphate buffer A, and 3.4 mL/g COD phosphate buffer B were fed to both AnMBRs as influent. The composition of both micro- and macronutrients, and both buffer solutions were adopted from the research conducted by Garcia Rea et al. (2022), and are presented in Table 1 along with the details of the applied concentrations of phenol and p-cresol.

The experiment consisted of two phases, differentiated by the concentration of the nano-magnetite added to the AnMBR-M. In Phase 1, AnMBR-M was supplemented with a concentration of 40 mmol/L Fe_3O_4, resulting in an average magnetite-to-biomass ratio of 6.67 mmol magnetite/g VSS, adopting the ratio from literature (He et al., 2019; Jung et al., 2022; Yan et al., 2018). Prior to the initiation of Phase 1, the biomass was acclimatized and achieved a conversion rate of 5.5 mg/(gVSS·d) for both phenol and p-cresol, applying an influent concentration of 200 mg/L, and an influent flow rate of 1 L/d. Prior to Phase 2, the biomass from AnMBR-C was divided into two parts, and then AnMBR-M was emptied and refilled with half of the biomass from AnMBR-C. Additionally, the AnMBR-M was supplied with 20 mmol/L Fe_3O_4, maintaining the same magnetite-to-biomass ratio from Phase 1. Following these steps, both reactors were replenished with demineralized water to restore the working volume to 6.25 L, as per the initial conditions. Because, due to the redistribution, the biomass (VSS) concentration was approximately halved at the start of Phase 2, the influent flow rate was decreased to 0.4 L/d to prevent biomass inhibition before being increased stepwise back to 1 L/d. After the flow rate reached 1 L/d, the concentration of the influent phenolic concentration was increased again step by step up to 4000 mg/L.

Table 1

2.2. Specific methanogenic activity assay (SMA)

SMA tests were performed once in each phase, i.e., in stage 1e and 2d (Table 1). The biomass samples were taken from both AnMBRs on day 62 for Phase 1, and on day 18 for Phase 2. In Phase 1, six serum bottles, each with a volume of 150 mL, were divided into two sets of three bottles each. Each bottle was inoculated with 2 gVSS/L of biomass, fed with 1 gCOD/L of acetate, and filled with demineralized water up to a liquid working volume of 90 mL. The bottles were then sealed with rubber stoppers and flushed with N_2 gas for 5 min. The gage pressure of the bottles was monitored with a pressure meter twice a day to assess the methane production between the two time intervals.

During Phase 2, the headspace pressure increase during the SMA test was measured using Oxitop pressure heads (Xylem Analytics, the Netherlands). In order to accommodate the Oxitop connector, 350 mL Schott Duran serum bottles were utilized, while maintaining a working volume of 90 mL.

2.3. Batch experiments assessing phenolics conversion using different inoculum biomass

Two series of batch experiments were conducted, using different inoculum sources. The first series was inoculated with non-adapted biomass, neither to phenol nor magnetite. The experiments were performed in 250 mL Schott Duran serum bottles with a working volume of 200 mL. The biomass was identical to the one used to inoculate the AnMBRs in Phase 1. The degradation of each phenol, p-cresol, benzoate, and propionate was investigated individually in the absence and presence of nano-magnetite. Each compound was supplied as the sole carbon source in the batch bottle. The initial concentration for each the compounds was 1 g COD/L. In addition, 4.4 mL buffer A, 7.8 mL buffer B, 1.5 mL micronutrient solution, and 3 mL macronutrient solution were added following the recipe in Table 1. The bottles were flushed with N_2 for 5 min before being incubated in a Mettler incubator (Germany) under a shaker speed of 180 RPM and a temperature of 35°C. Concentration of phenol and p-cresol was measured daily with gas chromatography as explained in 2.8.

The second series of batch experiments was performed using adapted biomass as inoculum, also in 250 mL Schott Duran serum bottles with a working volume of 200 mL. The serum bottles were divided into a control group (C) and a magnetite-supplemented group (M). Each group was a set of three bottles, serving as triplicate. Each bottle was inoculated with biomass directly taken from the corresponding AnMBR on day 87 of Phase 2, with AnMBR-M biomass already containing 20 mmol/L Fe_3O_4. The experiment followed a fed-batch procedure, in which consecutive phenol batch feedings were performed. All groups were provided with an initial concentration of 200 mg/L of phenol in the first feeding. When the phenol was depleted, fresh phenol solution containing 5.8 mL buffer A, 8.9 mL buffer B, 2.0 mL micronutrients and 3.9 mL macronutrients was added into the bottle. The initial phenol concentration for the second and third feeding was 1100 mg/L. The experiment was conducted in a Mettler incubator (Germany) under a shaker speed of 180 RPM and a temperature of 35°C. Phenol concentration was periodically measured with gas chromatography (see 2.8).

2.4. Statistical t-test

Statistical t-tests were conducted to compare the significance of the magnetite influence on the methane production rate during the continuous AnMBR experiment and the batch experiments. When comparing the time series data sets with increasing trends, the data sets was detrended by reducing the n + 1 value with value n. This detrending method was performed to avoid the biased mean value because the mean value increased over time.

2.5. DNA extraction and microbial community analysis

Biomass samples were extracted from the reactors and centrifuged at 18500 ×g for 10 mins. The supernatant was decanted, and approximately 5 g of centrifuged biomass was stored in a freezer at −80°C. Before DNA extraction, the frozen biomass was thawed in a 4°C fridge. The DNA samples were obtained using a DNA extraction kit (FastDNA Spin Kit for Soil, MP Biomedicals, USA), following the manufacturer's instructions for the extraction method.

The amplification of DNA (specifically the 16S rRNA gene) was performed on the Illumina Novaseq 6000 platform, facilitated by Novogene. The primer sets 341 F [(5′- 3′) CCTAYGGGRBGCASCAG] and 806 R [(5′- 3′) GGACTACNNGGGTATCTAAT] were utilized to amplify the hypervariable regions V3-V4. The polymerase chain reaction (PCR) procedures were conducted using Phusion ® High-Fidelity PCR Master Mix, manufactured by New England Biolabs.

The reads underwent quality filtering and denoising, and the amplicon sequence variations (ASVs) were determined using the DADA2 plugin (Callahan et al., 2016). Chimeras were removed using the *consensus* approach. The taxonomic classification of the representative sequences of ASVs was conducted using the "classify-consensus-vsearch" plugin (Rognes et al., 2016) with the SILVA (132) database as a reference. The representative sequences were aligned using the MAFFT technique (Katoh and Standley, 2013), and a phylogenetic tree was built using FastTree (Price et al., 2010). The feature table and tree were transferred to the R environment. The vegan library (Oksanen et al., 2013) was used to conduct PERMANOVA analysis between reactor operation stages. The visualization of the abundance and the tree was carried out using the phyloseq library (McMurdie and Holmes, 2013). The sequences in this study could be accessed in the NCBI database under the accession number PRJNA1131114.

The biomass functional potential was inferred from 16S rRNA amplicons with PICRUSt2 (Douglas et al., 2020). Per-ASV KEGG Ortholog (KO) copy numbers were predicted by hidden-state reconstruction, and sample-level KO profiles were obtained. An a priori KO panel was compiled for hydrogen/formate-mediated interspecies transfer (IHT/IFT) and for direct interspecies electron transfer (DIET) from the literature and the KEGG database, encompassing a total of 28 KOs. Differential enrichment of these KO markers between Control and Magnetite conditions was tested with ALDEx2 (Fernandes et al., 2013, 2014), a compositional method recommended for PICRUSt2-derived metagenomes, by supplying the unnormalized PICRUSt2 KO counts to the ALDEx2 workflow, generating Dirichlet-multinomial Monte-Carlo instances, applying centered log-ratio transformation, and assessing group differences with Welch's t-tests adjusting p-values with Benjamini–Hochberg FDR. Adjusted p-values and ALDEx2 effect sizes on the CLR scale are reported to identify KOs enriched in each condition.

2.6. Adsorption experiment

The possible adsorption of phenol and p-cresol to magnetite was researched, applying different concentrations of phenolics in the presence of 20 mmol/L nano-magnetite. The experiment was conducted by preparing 50 mL solution in 60 mL serum bottles containing either phenol or p-cresol with concentrations of 50, 100, 200, 300, and 500 mg/L. Each bottle was prepared in duplicates. At time zero, 20 mmol/L nano-magnetite was supplied into the bottles. The bottles were placed in a Mettler incubator (Germany) at a temperature of 35°C and a shaking speed of 180 RPM. Samples were collected before the addition of the nano-magnetite and once every hour after the nano-magnetite addition. The experiment was concluded when the concentration of phenolics reached equilibrium.

Based on the collected data, adsorption parameters were calculated for Langmuir and Freundlich isotherms. Furthermore, using the parameters from the best-fit isotherm model, the adsorbed amount of phenolic compounds was predicted. The prediction was performed for all the concentrations of phenolic compounds in the feed that were used in AnMBR experiments. During the calculation, some simplifications were made. Firstly, since adsorption predictions were performed up to phenolics concentration of 4000 mg/L, it was assumed that the calculated parameters are valid under initial concentrations higher than 500 mg/L, which was the highest concentration in the AnMBR experiment influent. Secondly, the adsorption percentage was calculated under the assumption that the nano-magnetite's surface is still free from adsorbates. Thirdly, the calculations were performed for each compound, neglecting any potential interactions between the compounds or competitive adsorption.

2.7. Biomass conductivity measurements

Biomass sample was centrifuged at 8000 x g at 20°C. Conductivity measurements were performed on ~1 g centrifuged biomass samples. The measurements were carried out using a two-probe setup equipped with gold-coated electrodes adopting the method described by Zhao et al. (2016). Samples were applied on the 5 μm gap between the two electrodes. A voltage ramp ranging from 0.3 V to −0.3 V was applied to the sample in increments of 0.025 V with a power supply unit NGU401 (Rohde & Schwarz, The Netherlands), and then the generated current was collected. Finally, the biomass conductivity was calculated following Zhao et al. (2016).

2.8. Other analytical methods

The quality of the effluent and that of the mixed liquor were monitored throughout the experiment. The measurement of TSS and VSS was performed following Standard Methods (APHA, 1998). Total COD and soluble COD were measured with HACH test kits (HACH, London, Ontario, Canada). Total Fe concentrations were measured with Merck test kits (Merck, Darmstadt, Germany).

The phenol, p-cresol, and volatile fatty acid concentrations were measured with gas chromatography Agilent 19091F-112 (25 m × 320 μm × 0.5 μm) column and an FID detector (Agilent 7890 A). Before analysis, a 5 mL sample was filtered with a 0.45 μm Whatman filter paper. 750 μL filtered sample was added together with 750 μL pentanol (300 mg/L) and 10 μL formic acid (purity > 99 %) into the final GC vial. The sample injection volume was 1 mL. Helium was used as a carrier gas with a total flow rate of 67 mL/min and a split ratio of 25:1. The temperature of the GC oven was set to rise from 80°C to 180°C over 10.5 min. The injector and detector temperatures were 80°C and 240°C, respectively. The total run time was 15.5 min.

Methane content in the biogas was measured using GC Agilent 7890 (Agilent Technology, USA) equipped with an HP-PLOT Molesieve (19095P-MS6, 60 m × 530 μm × 20 μm) column and a thermal conductivity detector (200°C). The biogas sample injection volume was 10 mL. Helium was used as a carrier gas with a flow rate of 10 mL/min. The oven temperature was set at 40°C for 6 min and was increased to 100°C with a gradient of 25 °C/min.

A high-performance liquid chromatograph (Shimadzu, Japan) was used to monitor the concentration of the intermediate compounds 4-hydroxybenzoic acid and benzoate. The column used was a Macherey-Nagel NUCLEODUR 100–3 CN-RP, 3 μm, 125 × 2 mm (Germany). The column temperature was 30°C. The sample was eluted with a mixture of 0.1 % formic acid in acetonitrile and 0.1 % formic acid in ultrapure water with a total flow of 0.4 mL/min. The composition of the eluent mixture followed a gradient step as mentioned in Table S1. The sample injection volume was 10 μm. A UV-Vis detector was used at ambient temperature with wavelengths 205 nm for channel 1 to detect benzoate and 269 nm for channel 2 to detect phenol, p-cresol, and 4-hydroxybenzoic acid.

3. Results and discussion

3.1. Anaerobic membrane bioreactor (AnMBR) operation

3.1.1. Phase 1

The continuous flow and batch experiments described in the materials and methods (2.1) employed an average magnetite-to-biomass ratio of 6.67 mmol magnetite/g VSS, in agreement with the literature (He et al., 2019; Jung et al., 2022; Yan et al., 2018). It was decided to adopt this ratio in these experiments, hypothesizing that the interaction biomass-magnetite is of higher importance than the absolute magnetite concentration. Notably, the applied biomass concentration in Phase 1 of the AnMBR experiment was twice the value reported in the literature. Therefore, the resulting nano-magnetite concentration in Phase 1 of the AnMBR experiment was 40 mM instead of the 20 mM as in the cited references (He et al., 2019; Jung et al., 2022; Yan et al., 2018).

The operational results of the AnMBRs in Phase 1 are summarized in Fig. 2. The organic loading rate (OLR) was increased stepwise by increasing the concentration of both phenol and p-cresol from 200 mg/L to 900 mg/L in Phase 1. As shown in Fig. 2a, the contribution of the phenolic compounds to the OLR increased from 23 % to 69 %, along with the increase in the concentration of phenol and p-cresol in the feed composition. In addition, TMP data indicate that there was no significant accumulation of membrane fouling in both AnMBRs throughout Phase 1 (See Figure S1, Supplementary material).

From the start of Phase 1 until day 66, both AnMBRs had similar daily methane production (Fig. 2a), which increased whenever the concentration of phenol and p-cresol was increased, following the trend of the OLR. A *t*-test was performed to evaluate the similarities of the daily methane production between AnMBR-C and AnMBR-M from day 2 to day 66. The result indicated that there was no significant difference in the daily methane production between both AnMBRs ($t(45) = 0.2418$, $p < 0.05$). Therefore, the statistical test suggested no effect of nano-magnetite addition on the methane production rate in Phase 1. On day 62, an SMA assay using acetate as the substrate was conducted to determine the maximum acetotrophic methanogenic activity of the biomass from both AnMBRs. The assay showed SMA values of 0.76 ± 0.19 gCOD-CH_4/(gVSS·d) and 0.52 ± 0.01 gCOD-CH_4/(gVSS.d) for AnMBR-C and AnMBR-M, respectively. A statistical test suggested that the acetotrophic methanogenic activity in AnMBR-M was lower than in AnMBR-C ($t(2) = 4.5143$, $p < 0.05$). Even though the SMA of AnMBR-M biomass was lower than that of AnMBR-C, both AnMBRs had a similar daily methane production rate. The findings suggest that acetotrophic methanogenesis was not the rate-limiting step in the phenol and p-cresol degradation, and that growth and/or presence of acetotrophic methanogens was negatively affected by nano-magnetite in Phase 1. The somewhat lower methanogenic activity may explain the retarded p-cresol conversion performance in AnMBR-M at the end of Phase 1. After ring splitting, the main intermediate in p-cresol degradation, benzoate, is degraded through β-oxidation, producing acetate and butyrate (Nobu et al., 2015). A possible accumulation of intermediate compounds may reduce the thermodynamic feasibility of benzoate degradation, potentially affecting p-cresol degradation.

Moreover, AnMBR-M was found to have a lower methane yield than AnMBR-C in Phase 1 ($t(27) = 2.2530$, $p < 0.05$). The lower methane yield could not be attributed to Fe(III) reduction to Fe(II), because the total Fe concentration in AnMBR-M permeate was lower than in AnMBR-C for most of Phase 1 (Fig. 2d). Therefore, the possibility of increased electron capture by Fe (III) in AnMBR-M can be ruled out. This suggests that either more electrons in AnMBR-M were directed toward anabolic processes rather than methane production through catabolism, or electrons were used in non-identified reduction processes in the medium or sludge.

A small but clear difference was observed in the conversion of the phenolic compounds between AnMBR-C and AnMBR-M at the end of Stage 1. Both AnMBRs maintained a 100 % conversion of phenol and p-cresol up to day 50 in Stage 1d (Fig. 2b). However, small amounts of p-cresol started to be present in the permeate of both AnMBRs during the period of Stage 1d, indicating that the biomass

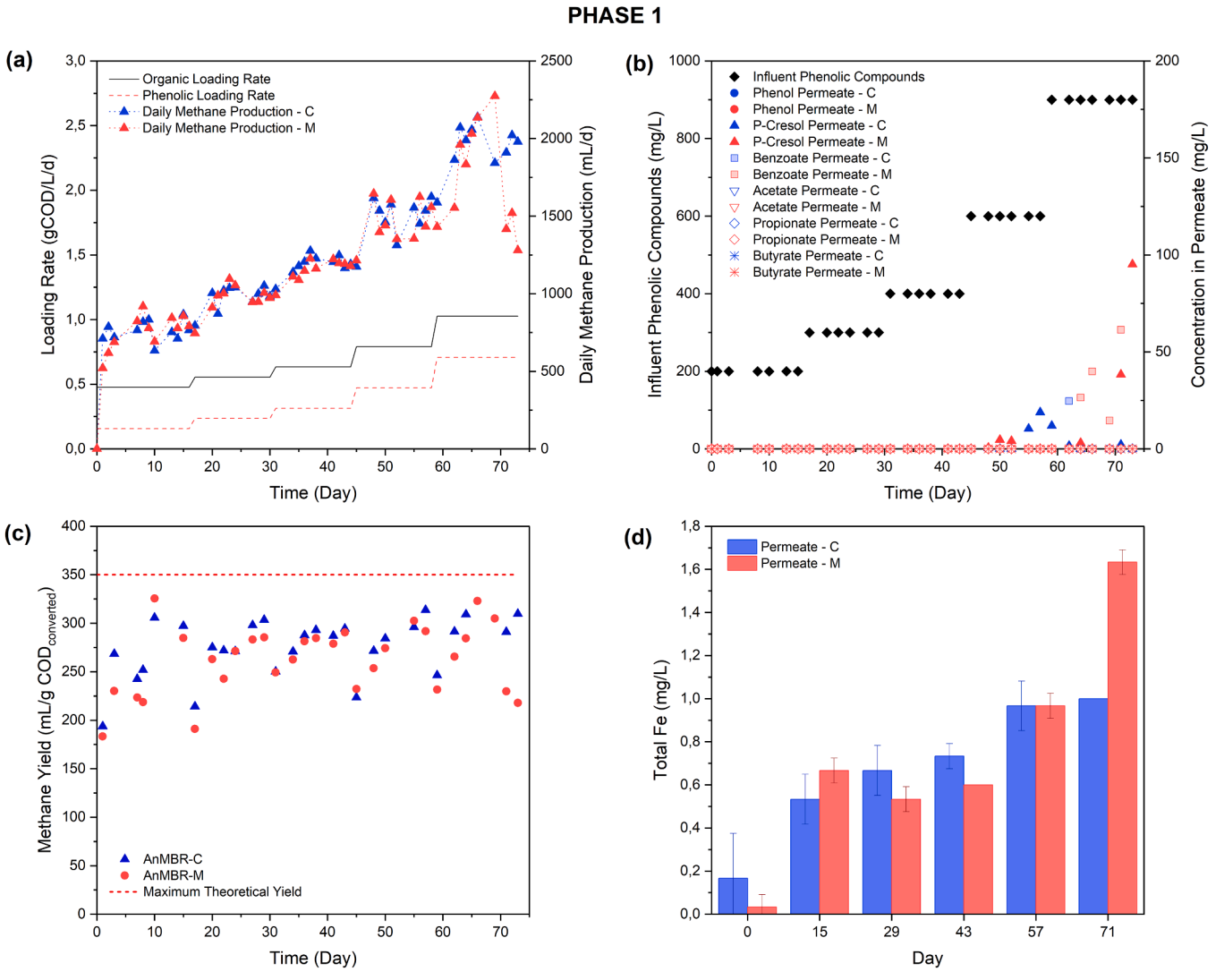

Fig. 2. Operation of AnMBR-C and AnMBR-M in Phase 1. a) loading rate and methane production rate, b) influent and permeate concentrations, c) methane yield, and d) total Fe concentrations in permeate. AnMBR-M was supplemented with 40 mmol/L Fe_3O_4. "Phenolic loading rate" in graph (a) represents the organic loading rate collectively contributed by phenol and p-cresol. In graph (b), "Influent phenolic compounds" represent the concentration of each phenol and p-cresol in the influent (left y-axis). The other parameters in graph (b) were measured in the permeate and belong to the right y-axis.

was on the verge of its conversion capacity. In Stage 1e, the concentration of phenol and p-cresol was increased from 600 mg/L to 900 mg/L. The increased OLR caused the benzoate to accumulate in both AnMBRs' permeate. However, contrary to AnMBR-C where the conversion efficiency recovered soon, the benzoate kept accumulating in AnMBR-M, reaching 61.4 mg/L. It was then followed by the accumulation of unconverted p-cresol in AnMBR-M's permeate, up to 95.2 mg/L. This indicates that the OLR exceeded AnMBR-M's conversion capacity of phenolics. It must be highlighted that phenol conversion was maintained at 100 % even when benzoate and p-cresol accumulated in AnMBR-M. This observation suggested that phenol was more easily degraded than p-cresol, in line with the previously reported observations in the literature (Chi et al., 2021; García Rea et al., 2020).

Phase 1 was terminated to prevent inhibition of the biomass. Observed results indicated that 40 mmol/L nano-magnetite failed to enhance the degradation of p-cresol and did not enhance the methane production rate. Afterward, the AnMBR-M biomass was stored, and AnMBR-C biomass was divided into two portions to reinoculate both AnMBRs before the start of Phase 2.

3.2. Phase 2

The concentration of Fe_3O_4 in AnMBR-M was reduced from 40 mmol/L to 20 mmol/L in Phase 2 to adopt the same magnetite concentration as the referred literature (He et al., 2019; Jung et al., 2022; Yan et al., 2018). Since the biomass concentration was halved the magnetite/VSS ratio was maintained at 6.67 g/g. Similar to Phase 1, there was no substantial membrane fouling accumulation in both AnMBRs throughout Phase 2 (See Figure S1, Supplementary material). In this phase, the contribution of the phenolic compounds to the OLR increased from 69 % to 91 %, making the phenol and p-cresol the dominant part of the influent COD. Similarly

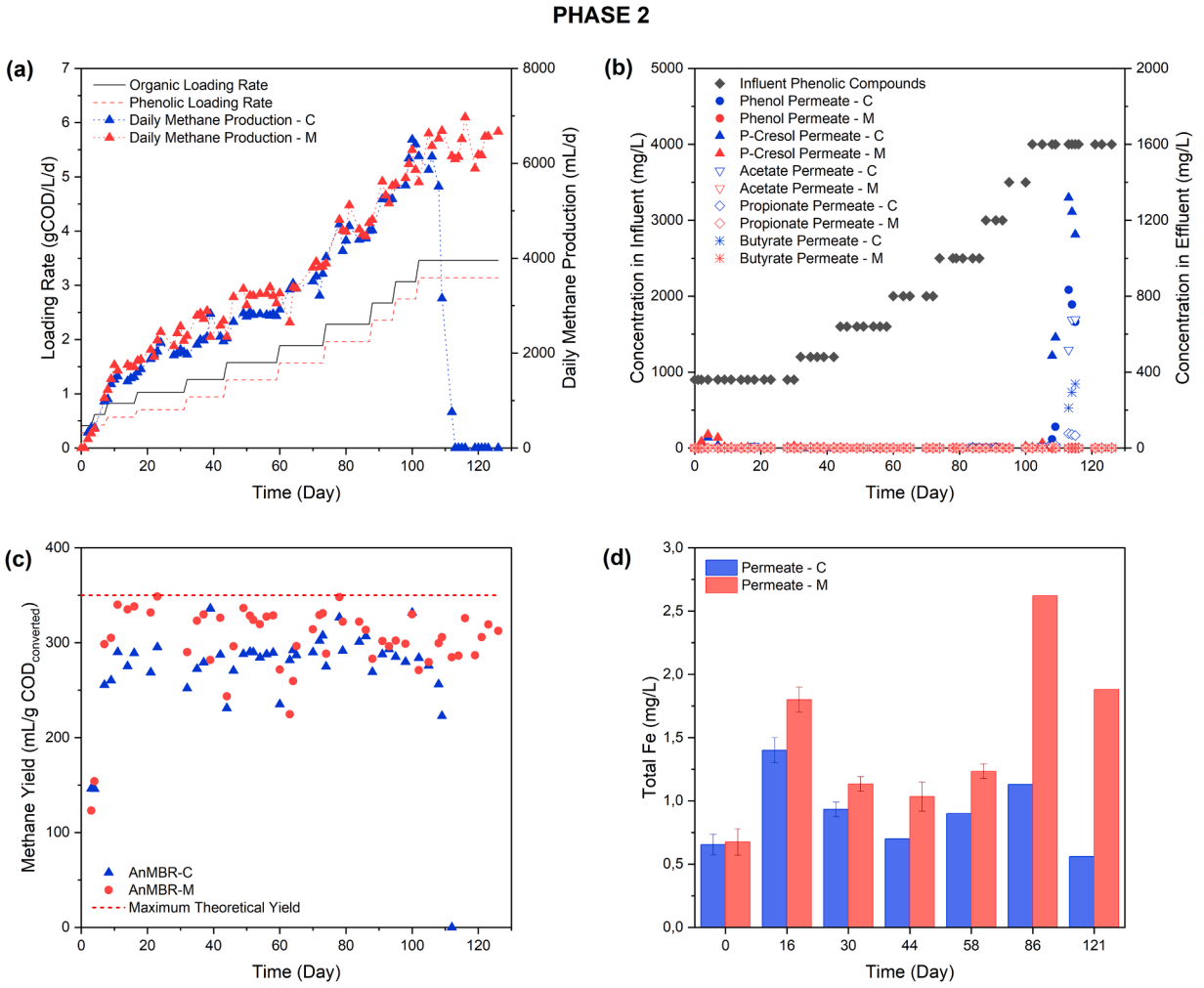

Fig. 3. Operation of AnMBR-C and AnMBR-M in Phase 2. a) loading rate and methane production rate, b) influent and permeate concentrations, c) methane yield, and d) total Fe concentrations in permeate. AnMBR-M was supplemented with 20 mmol/L Fe_3O_4. "Phenolic loading rate" in graph (a) represents the organic loading rate collectively contributed by phenol and p-cresol. In graph (b), "Influent phenolic compounds" represent the concentration of each phenol and p-cresol in the influent (left y-axis). The other parameters in graph (b) were measured in the permeate and belong to the right y-axis.

to Phase 1, the daily methane production rate in both AnMBRs in Phase 2 followed the OLR increase, and then remained stable under the same OLR (Fig. 3a). The trend was consistent until Stage 2j on day 101. During Stage 2c to Stage 2 f, AnMBR-M produced an average of 300 mL/d more methane than AnMBR-C, suggesting that nano-magnetite might have enhanced the methane production rate. However, statistical analysis concluded no differences between both reactors ($t(68) = 0.1571$, $p < 0.005$). In agreement with Phase 1, half dosage of nano-magnetite also did not enhance the methane production rate.

An SMA assay was conducted to compare the methanogenic activity of the biomass between the two AnMBRs after two weeks of operation. Sludge samples were taken on day 18, and SMA assays revealed values of 0.67 ± 0.05 gCOD-CH_4/(gVSS·d) and 0.63 ± 0.03 gCOD-CH_4/(gVSS·d) for AnMBR-C and AnMBR-M, respectively. These values did not differ significantly ($t(9) = 1.8432$, $p < 0.05$), confirming that acetotrophic methanogenesis was not enhanced by nano-magnetite as observed in Phase 1. Despite that, the increased SMA of AnMBR-M biomass compared to that in Phase 1 suggested that 20 mmol/L nano-magnetite dosage did not negatively impact acetotrophic methanogenic activity, in contrast to the negative effects observed using 40 mmol/L.

The methane yield of AnMBR-M was on average 42 mL/g $COD_{converted}$ higher than AnMBR-C's methane yield until the end of Stage 2 f (day 60). After that, the gap between the methane yields of both AnMBRs started to diminish, which coincided with an increased total Fe concentration in AnMBR-M after day 60 (Fig. 2d). The higher total Fe concentration indicates that more electrons were captured by Fe(III), reducing the available electrons for methanogenesis in AnMBR-M. Nonetheless, AnMBR-M's methane yield was found to be higher than AnMBR-C's in Phase 2 ($t(39) = 5.814$, $p < 0.05$).

The effect of magnetite on methane production in the anaerobic degradation of phenol is conflictively cited in the literature. For example, Tang et al., (2021) reported that magnetite enhances both the methane yield and methane production rate. However, another study concluded that the yield is not affected; only the rate is enhanced by magnetite (Jung et al., 2022). Furthermore, in the study conducted by He et al. (2019), magnetite was found to enhance methane yield in some instances, but sometimes it even had a negative impact. In addition, they also reported that magnetite did not enhance either the hydrogenotrophic or acetoclastic methanogenesis rate, agreeing with the findings of this study. Magnetite was also reported to improve the methane yield in the anaerobic degradation of various types of substrate, including furfural, pre-treated waste activated sludge, and nitrogen heterocyclic compounds (Feng et al., 2022; He et al., 2022; Yang et al., 2024).

Thus far, there is no clear explanation why magnetite has different enhancement effects on methanogenesis. Magnetite is supposed to serve as an electron channeler for DIET mechanisms (Wang et al., 2021). Therefore, it should only affect the electron transport's kinetics, potentially enhancing the methane production rate, not the methane yield. Alterations in methane yield, for instance a decrease, can be expected when intermediate compounds are formed, or when alternative electron acceptors like oxygenated anions or oxidized metals are present (van Lier et al., 2008). Conversely, an increase in the methane yield can be expected when no intermediates accumulate or when the biomass yield per mass of converted substrate decreases. In this study, no intermediate compounds in AnMBR-C were detected during the period when the methane yield in AnMBR-M was higher. Therefore, it was hypothesized that the increased methane yield in AnMBR-M was related to a reduced biomass yield. This hypothesis was supported by the observation that VSS concentrations in AnMBR-M were lower than those in AnMBR-C during most of Phase 2 (see Figure S2, Supplementary material). Considering the fact that more total Fe ions were measured in AnMBR-M, and thus even less electrons were channelled to methanogenesis, the impact on the biomass yield must have been considerable. This finding suggests that nano-magnetite had a similar role to other stressors. As postulated by Muñoz Sierra et al. (2018), the presence of stressors promotes catabolic conversions to generate energy for intensified biomass maintenance, at the expense of microbial growth. Nevertheless, the observed higher total Fe concentration in AnMBR-M could be indicative of enhanced electron transfer between the syntrophic microbes. As reported in the literature, magnetite may be involved in a dissimilatory iron reduction-oxidation cycle, producing Fe(II) ions followed by re-oxidation to Fe(III) mineral that facilitate the transfer of electrons from acidogens to methanogens (Tang et al., 2021; Xu et al., 2019).

Regarding the phenolic compound conversion performance, both AnMBR-C and AnMBR-M fully degraded phenol and p-cresol up to Stage 2 g (2000 mg/L phenol and p-cresol in the influent). In the following stages up to Stage 2j, some VFAs started to be detected, indicating that both AnMBRs were operating near the maximum conversion capacity. Finally, p-cresol started accumulating rapidly in AnMBR-C in Stage 2k, followed by the accumulation of both phenol and volatile fatty acids. Unfortunately, benzoate concentrations could not be monitored throughout Phase 2 due to a technical problem with the HPLC unit. However, based on the observation in Phase 1, benzoate was expected to accumulate earlier than p-cresol. At the end of Phase 2, i.e. stage 2k, the methane production in AnMBR-C finally ceased, and its operation was stopped. In contrast, AnMBR-M still consistently degraded phenol and p-cresol with 100 % conversion and showed stable methane production before the experiment was terminated two weeks after the failure of AnMBR-C. The higher phenol (20.8 % more) and p-cresol efficiency (33 % more), as well as higher CH_4 daily production rate (85 % more) in AnMBR-M in stage 2k showed that AnMBR-M was able to handle a higher phenolic loading rate than AnMBR-C.

The finding in Phase 2 differed from Phase 1, where 40 mmol/L nano-magnetite was found to negatively impact the reactor's conversion performance. Since the ratio of magnetite to VSS concentration was the same in both phases (6.67 mmol Fe_3O_4/gVSS), it seems likely that magnetite dosage played a larger role than the ratio of magnetite to VSS concentration. Studies performed by others revealed that excessive dosage of conductive materials may cause oxidative stress resulting in the possible release of reactive oxygen species (ROS), which may decrease overall microbial activity (Guan et al., 2023; Lu et al., 2022). However, further studies are needed to verify the possible relationship between magnetite dosage and ROS production, particularly in the anaerobic degradation of phenolic compounds.

Previous studies that demonstrated enhancements in methane production during the anaerobic degradation of phenol with the addition of magnetite also employed a magnetite concentration of 20 mmol/L (He et al., 2019; Jung et al., 2022; Tang et al., 2021). The research of Tang et al. (2021) reported a concomitant enhancement of the phenol degradation rate. Another study confirmed that the optimal magnetite dosage for phenol degradation was in the range of 5–20 mmol/L, where concentrations higher than 30 mmol/L

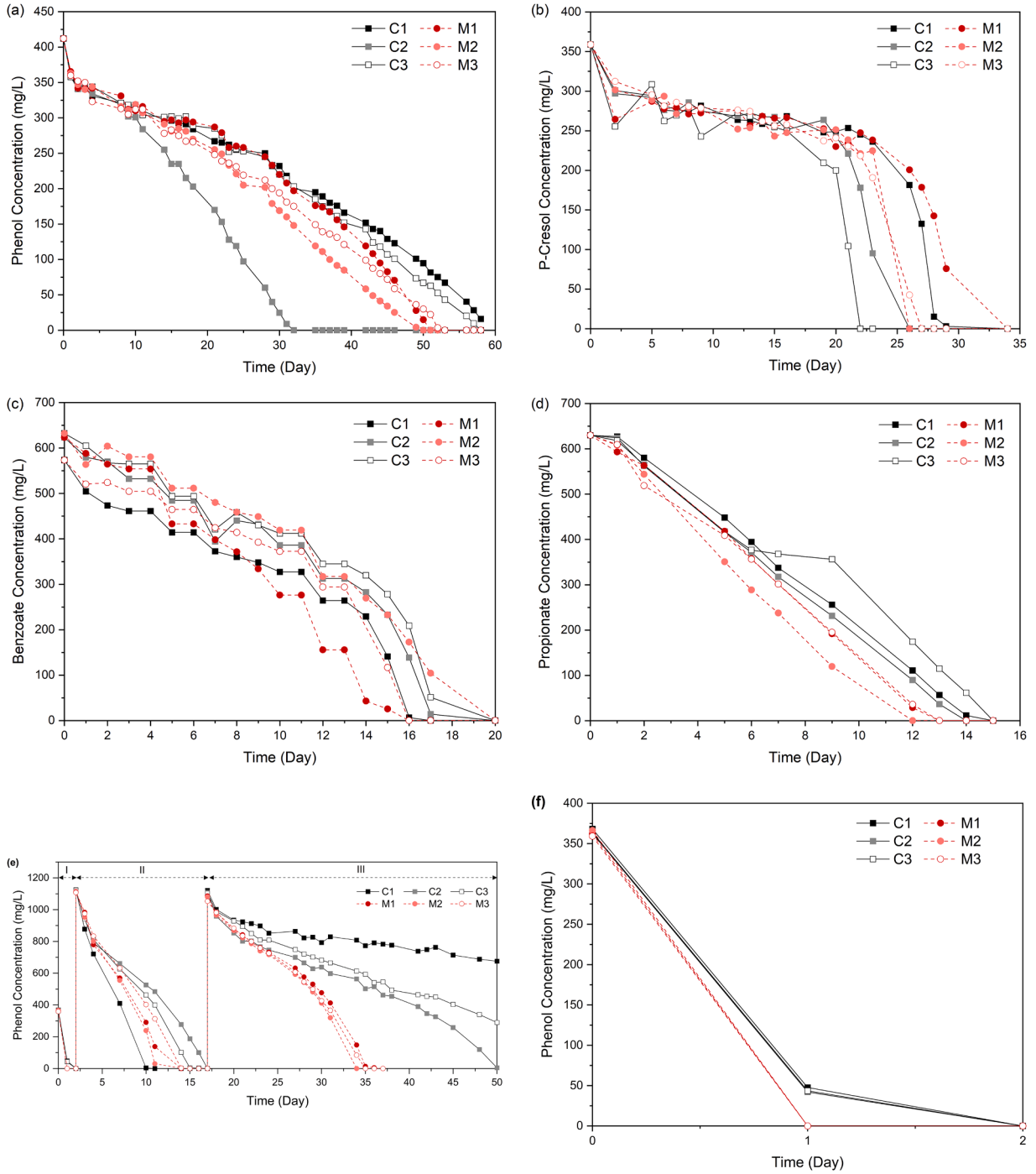

Fig. 4. C represents the control batch group inoculated with AnMBR-C's biomass, and M represents the batch group inoculated with AnMBR-M's biomass. When the phenol concentration in all bottles reached 0 mg/L, fresh phenol was injected into the bottle. I, II, and III represent the first, second, and third feeding, respectively. Each group was a set of triplicate batch bottles. Each triplicate was represented by numbers 1, 2, and 3. (a) The anaerobic degradation of a) phenol, b) p-cresol, c) benzoate, and d) propionate with biomass that was not adapted to either phenol or magnetite. (b) AnMBR-C's biomass was adapted to phenol, whereas AnMBR-M's biomass was adapted to both phenol and 20 mmol/L nano-magnetite. (c) The batch-in-sequence degradation of phenol with adapted biomass collected from the AnMBRs: e) The whole batch sequence, f) the zoomed result of the first feeding.

inhibited the CH_4 production rate (Jung et al., 2024). These studies support the prevalence of inhibitory nano-magnetite concentrations in Phase 1, contrary to the positive effect observed in Phase 2.

In addition to the previously mentioned optimal magnetite dosage of 20 mmol/L, Ma et al. (2021) and Guan et al. (2023) identified 200 mg/L (equivalent to 0.86 mmol/L) of magnetite as the optimal concentration, after comparing several dosages of magnetite (0 – 600 mg/L). These studies reported that a higher or lower dosage than 200 mg/L magnetite resulted in reduced methane production and reduced COD removal efficiency.

The differences in reported optimum magnetite dosages in the literature may also be influenced by differences in the types of wastewater studied (see Table S3, Supplementary materials) and by differences in the presence of electrochemically active microorganisms. Ma et al. (2021) examined real coal gasification wastewater, which is characterized by the presence of various toxic and inhibitory compounds, whereas Guan et al. (2023) studied synthetic high-salinity organic wastewater with glucose as the carbon source and a controlled salinity of 30 mg/L. The presence of more severe stressors in wastewaters could have a synergistic effect on microbial metabolism, rendering the biomass more sensitive to additional inhibitory effects that could come from elevated magnetite concentrations. Therefore, for future studies or scale-up applications, it is recommended to refer to existing literature with similar experimental setups, particularly with regard to the type of wastewater, for guidance on determining the optimal magnetite dosage.

3.3. Batch experiments with different biomass adaptation

Based on the obtained results and literature reports, it was hypothesized that the negative effect of nano-magnetite on AnMBR-M's performance in Phase 1 was attributable to the dosage exceeding its optimum value. However, there is also a possibility that the microbes being able to use magnetite as an electron conduit in the degradation of phenolic compounds were still hardly present in Phase 1. Notably, the COD contribution from the phenolic compounds in the feed only amounted to 23 % at the start of Phase 1, while the rest of the COD consisted of acetate and butyrate. In addition, both the growth rate and growth yield of degraders of recalcitrant compounds, like phenolics, are relatively low, while the biomass requires a long acclimation period (Al-Asheh et al., 2021). Therefore, the biomass in Phase 1 was likely only limitedly enriched with phenol and p-cresol degraders. Consequently, a series of batch experiments was conducted to research the need for biomass adaptation to nano-magnetite conductive particles.

3.4. Batch experiments with non-adapted biomass

Fig. 4 shows the concentration profiles of phenol, p-cresol, benzoate, and propionate during anaerobic degradation, with and without nano-magnetite. Based on the slope of the concentration profiles, no noticeable enhancement in the degradation rates of phenol, p-cresol, and benzoate was observed with the addition of nano-magnetite (see Table S2, Supplementary materials). Although not substantial, phenol and p-cresol were degraded faster in the magnetite-supplemented triplicates than in two of the control triplicates. The observations suggested a subtle increase in the degradation rates of phenol and p-cresol facilitated by nano-magnetite, although the enhancement was not completely evident. In contrast, benzoate was degraded more slowly in the magnetite-supplemented triplicates than in two of the control triplicates. The latter results suggested a possible negative impact of nano-magnetite on the benzoate degradation rate. Additionally, the degradation rate of propionate was evidently enhanced by nano-magnetite, unlike that of the other compounds (Fig. 4d).

3.5. Batch experiment with adapted biomass

Due to the limited amount of available adapted biomass from the AnMBRs, the batch experiment was only conducted for phenol degradation (Fig. 4e,f). As presented in Fig. 4e, phenol was completely converted in the magnetite-supplemented triplicate on day 1, while there was still 50 mg/L remaining in the control group. From this observation, it can be derived that the magnetite-adapted biomass degraded phenol faster than the control biomass. The control biomass had a phenol degradation rate of 641 ± 0 mg phenol/(g VSS·day). Conversely, the magnetite-adapted biomass had a phenol degradation rate of at least 725 ± 6 mg phenol/(g VSS·day) (See Table S2). The actual value could be even higher because the phenol was already depleted during the first measurement.

The batch bottles were resupplied with fresh phenol to make an initial concentration of 1100 mg/L in the second feeding. Notably, the phenol degradation rate declined in both groups, likely due to the biomass being exposed to high phenol concentrations. This decline suggests that the high phenol concentrations inhibited the biomass activity. The phenol degradation rate decreased by 88 % in both groups to 82 ± 36 mg phenol/(g VSS·day) for the control triplicate and 82 ± 9 mg phenol/(g VSS·day) for the magnetite triplicate. A *t*-test showed that there was no significant difference between the degradation rates of the two groups ($t(2) = 0.3277$, $p < 0.05$).

In the third feeding, the phenol was again replenished to 1100 mg/L. Remarkably, the phenol degradation rate was distinctly reduced in both groups, but the reduction in the magnetite-supplemented triplicate was less than in the control triplicate. Compared to the second feeding, the degradation rate in the control triplicate further decreased by 78 % to 18 ± 7 mg phenol/(g VSS·day). In contrast, the degradation rate in the magnetite-supplemented triplicate was only reduced by 44 % to 46 ± 3 mg phenol/(g VSS·day). This observation indicates that magnetite-adapted biomass had a higher resistance towards inhibition by high concentrations of phenol. The enhanced electron transfer in AnMBR-M biomass likely accelerated the phenol conversion rate, enabling it to reach a concentration below the inhibitory level more quickly than AnMBR-C biomass. This finding may explain why AnMBR-M was able to sustain higher phenolic loadings than AnMBR-C, as discussed in Section 3.1.2.

3.6. Adsorption tests

A subsequent experiment was conducted to assess the possible contribution of adsorption of phenol and p-cresol onto 20 mmol/L magnetite. Results showed that the Freundlich isotherm fitted the adsorption measurements of both compounds somewhat better than the Langmuir isotherm ((Figure S3, Supplementary materials). The Freundlich coefficient (K_F) was 1.298×10^{-4} for phenol adsorption and 1.335×10^{-4} for p-cresol adsorption. The Freundlich exponent (n) was 1.576 and 1.384 for phenol and p-cresol adsorption, respectively.

Based on the calculated coefficients, the amount of phenol and p-cresol adsorption was predicted (Table S4). The calculated values

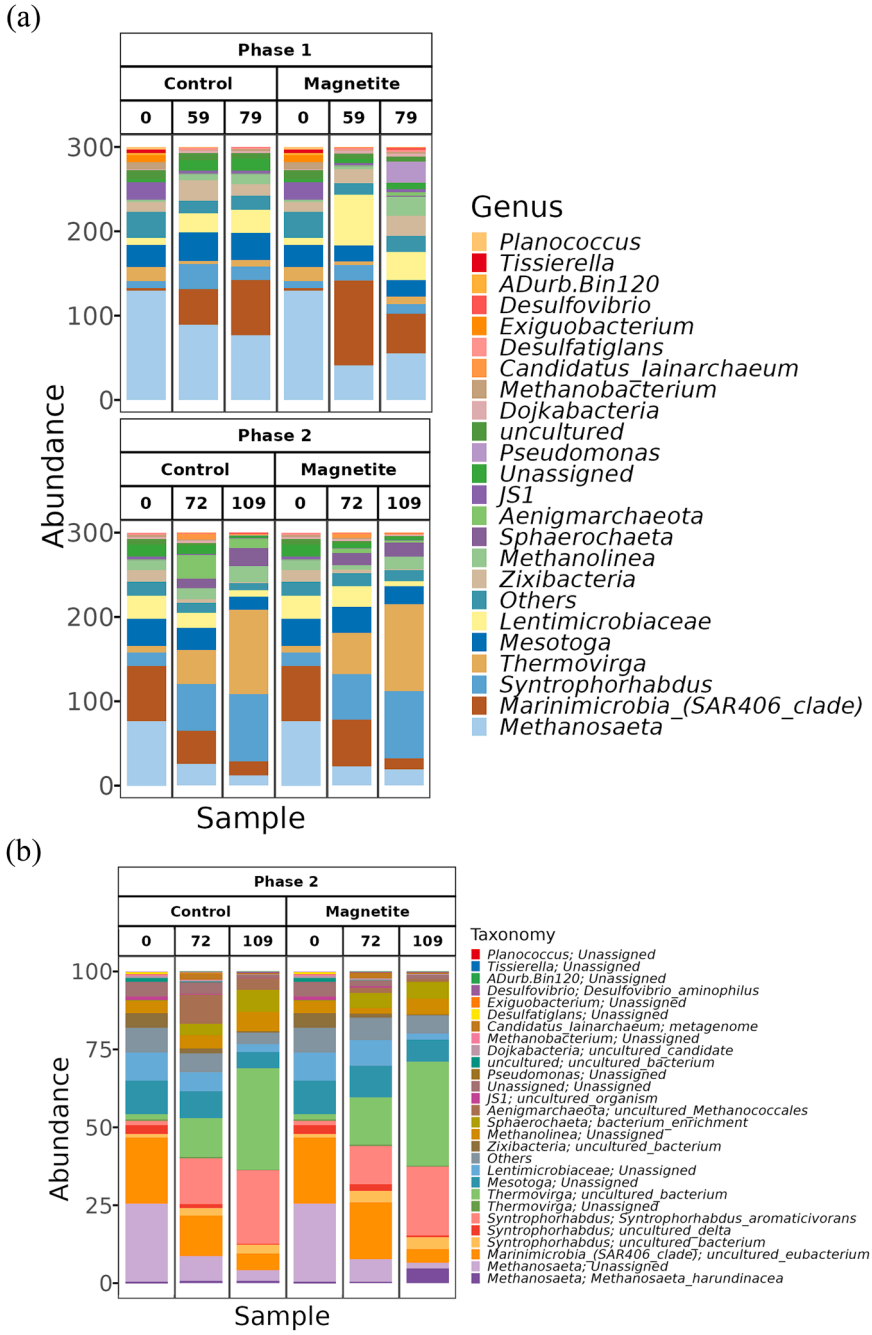

Fig. 5. Relative abundance of the microbial communities inside AnMBR-C and AnMBR-M biomass samples at the a) genus level and b) species level (only for Phase 2). Biomass was sampled on day 0, 59, and 79 for Phase 1 and day 0, 72, 109 for Phase 2. All sequencing was done in triplicates. Each bar represents the average of the triplicate values.

(see Table S4) might be overestimated due to the assumptions made for the calculation (see Section 2.5). Nonetheless, results provided insights into the contribution of phenolics adsorption to magnetite. Results showed that the adsorption potential of p-cresol was somewhat higher than that of phenol (Fig. 5). Based on these results, the calculated contribution of adsorption to the removal of phenol and p-cresol in batch experiments, applying an initial concentration of 4000 mg/L, was only 2.85 % and 5.92 %, respectively. Considering the possible overestimation in the calculation, this contribution is considered very modest. In the continuous flow AnMBR experiments, the phenolic concentrations in the completely mixed bulk liquid was considered to be equal to the permeate concentration, i.e., mostly 0 mg/L. Consequently, phenolics were negligibly absorbed to magnetite and it was assumed that the magnetite surface was still free of adsorbates. Therefore, it may also be assumed that the starting conditions regarding adsorbates to magnetite was similar for the batch experiments with biomass adapted to magnetite and non-adapted biomass, using newly added magnetite. In the batch experiments, possible phenolics adsorption cannot be excluded, owing to the high phenolics concentrations at the start. Therefore at the very start of the experiment, conversion rates in the presence of magnetite might be overestimated. Based on previous calculations (Table S4), an initial concentration of 200, 400, and 1110 mg phenol/L would lead to an adsorption of 8.2 %, 6.5 %, and 4.5 %, respectively, of the added phenol. For p-cresol, this would result in an adsorption of 12.9 %, 10.8 %, and 8.3 %, respectively, of the added amount. The calculated adsorbed amount of phenolics may have led to a biased observation regarding compound removal. However, considering that adsorption always reached equilibrium during the first hour, a possible contribution of adsorption during phenolics degradation that lasted several days was ignored.

Genes	Order of Magnitude					Significantly higher in	
	Phase 1		Phase 2		Process	Phase 1	Phase 2
K00533 (E1.12.7.2L)	0	1	0	0	IHT	M	C
K18008 (hydA)	0	1	0	0	IHT	M	C
K00437 (hydB)	0	1	0	0	IHT	M	C
K08350 (fdnI)	0	0	0	0	IFT	~	~
K08349 (fdNH)	0	0	0	0	IFT	~	~
K08348 (fdnG)	0	3	0	0	IFT	M	~
K00127 (fdoI, fdsG)	2	8	4	3	IFT	M	C
K00126 (fdsD)	0	0	0	0	IFT	M	~
K00123 (fdoG, fdhF, fdwA)	120	120	98	104	IFT	~	M
K00124 (fdoH, fdsB)	34	37	29	29	IFT	M	~
K00122 (FDH)	1	1	0	0	IFT	M	C
K22340 (hylC)	0	1	0	0	IFT	M	M
K22339 (hylB)	0	0	0	0	IFT	M	M
K22338 (hylA)	0	0	0	0	IFT	M	C
K22341 (fdF2)	6	4	1	0	IFT	C	C
K00125 (fdhB)	10	12	7	7	IFT	M	~
K22015 (fhdF)	0	0	3	3	IFT	C	C
K00297 (metF, MTHFR)	23	25	36	36	SAO	M	~
K01938 (fhs)	13	10	21	22	SAO	C	M
K15022 (fdhB)	4	4	1	1	SAO	C	~
K05299 (fdhA)	43	33	18	20	SAO	C	M
K00198 (cooS, acsA)	19	17	29	29	SAO	C	~
K14138 (acsB)	4	4	12	13	SAO	~	~
K00197 (cdhE, acsC)	19	16	29	29	SAO	C	~
K00194 (cdhD, acsD)	17	15	17	17	SAO	C	~
K15023 (acsE)	4	3	13	13	SAO	C	~
K02650 (pilA)	12	20	18	19	DIET	M	~
K02651 (flp, pilA)	1	1	0	0	DIET	M	~

Fig. 6. Heat map of the order of magnitude of gene abundance predicted with KEGG functions. The "Process" column indicates the process related to the gene, where IHT is interspecies hydrogen transfer, IFT is interspecies formate transfer, SAO is syntrophic acetate oxidation, and DIET is direct interspecies electron transfer. The two columns on the right side of the graph show in which AnMBR the gene was found to be significantly more abundant, where "M" means AnMBR-M, "C" means AnMBR-C, and "~" means no significant difference was observed.

3.7. Microbial community analysis

Since non-adapted biomass was used to inoculate both AnMBRs in Phase 1 as well as the reactors in the batch experiments, the microbial community composition across these experiments is presumed to be the same. As illustrated in Figure S4, there was a small presence of *Syntrophomonas* in the non-adapted biomass (0.0026 ± 0.0005 %). The presence of electrogenic *Syntrophomonas* may explain the enhanced propionate degradation by nano-magnetite in Section 3.2.1, through syntrophic propionate oxidation (Sun et al., 2023).

Permutational multivariate analysis of variance (PERMANOVA) concluded that the microbial community of AnMBR-C was statistically different from AnMBR-M ($p < 0.05$). Fig. 5a indicates that the microbial community was dominated by four genera in Phase 1, covering approximately 60 % of all genera present. Those genera were *Methanosaeta*, *Marinimicrobia (SAR406)*, *Lentimicrobiaceae, and Mesotoga*. *Lentimicrobiaceae* was reported to be carbohydrate fermenters and acetate-oxidizing bacteria and capable of handling saline environments (Mazioti et al., 2021; L. Sun et al., 2016). *Marinimicrobia* (SAR406) is categorized as a marine bacteria, also found in saline conditions (Yilmaz et al., 2016).

In Phase 1, the relative abundance of *Mesotoga* exhibited a decline in the presence of nano-magnetite. *Mesotoga* was reportedly found in a relatively high abundance in phenol-degrading digesters and was proposed to contribute to the syntrophic acetate oxidation (SAO) pathway (Jung et al., 2022). In accordance with the relatively lower abundance of *Mesotoga* in AnMBR-M compared to AnMBR-C, the KEGG functions prediction shows that the genes for the SAO pathway (*metF, fhs, fdhA, acsA, acsC, acsD, and acsE*) were also significantly higher in AnMBR-C than in AnMBR-M, as shown in Fig. 6 (Kim et al., 2024) (for the complete comparison, see Figure S7a, Supplementary materials).

Similar to *Mesotoga*, the relative abundance of *Syntrophorhabdus* was also lower in AnMBR-M in Phase 1. *Syntrophorhabdus* was identified as the microorganism responsible for degrading phenol and p-cresol (Garcia Rea et al., 2022). However, it was present in relatively low quantities in both AnMBRs, i.e. 6.1 ± 0.9 % in AnMBR-C and 3.7 ± 0.3 % in AnMBR-M. The lower abundance of *Syntrophorhabdus* in AnMBR-M suggested that excessive magnetite dosage had a negative impact on their growth, and this might be one of the reasons for the lower p-cresol conversion performance in AnMBR-M. These results are also supportive for the presumed lower abundance of phenol and p-cresol degraders in the batch experiments described in Section 3.2.1.

In contrast with *Syntrophorhabdus*, *Methanolinea,* a hydrogenotrophic methanogen, was enriched in AnMBR-M (7.6 ± 0.1 % compared to 3.9 ± 0.7 % in AnMBR-C). *Methanolinea* was suggested to be involved in DIET for their enrichment in the GAC-supplemented anaerobic reactor and in microbial electrolysis cells (Lee et al., 2016).

The most striking difference between the two AnMBRs at the end of Phase 1 was the relatively high abundance of *Pseudomonas* (8.3 ± 1.9 %) in AnMBR-M, which is reported to be an electrogenic bacterium, capable of anaerobically oxidizing volatile fatty acids at the anode of a microbial fuel cell (Freguia et al., 2010). In addition, *Pseudomonas* spp. is suggested to be involved in the DIET pathway for VFAs conversion when conductive materials are present (Hashemi et al., 2022). This suggests the possible DIET stimulation between *Pseudomonas* spp. and *Methanolinea*, which was also enriched in AnMBR-M, and was previously reported to be involved in DIET with *Geobacter* (Lee et al., 2016). Moreover, predicted KEGG functions show that *pilA* gene was enriched in AnMBR-M in Phase 1 (see Fig. 6), supporting the suggested DIET stimulation (Kim et al., 2024). However, despite that such DIET stimulation might have been established, it did not help in enhancing p-cresol conversion performance in AnMBR-M, as shown by the accumulation of benzoate and p-cresol (Fig. 2). Possibly, this was due to the inhibitory effect of an excessive magnetite dosage, which resulted in lower availability of *Syntrophorhabdus* as the main p-cresol degraders. Moreover, anaerobic VFA oxidation was not the rate-limiting factor in p-cresol conversion, as shown by its much higher rate than the p-cresol conversion rate in Table S2 (Supplementary materials).

Unlike in Phase 1, there was no noteworthy difference between the microbial community of the two AnMBRs in Phase 2 ($p < 0.05$). The PERMANOVA analysis concluded that the increase in the phenol concentration in the feed had a greater influence on the development of the microbial communities than the addition of magnetite.

In both reactors, the development of the microbial community resulted in the dominance of *Syntrophorhabdus* and *Thermovirga*, which comprised about 60 % of the total population. Garcia Rea et al. (2022) also reported a similar observation in which *Syntrophorhabdus*, *Thermovirga*, and *Methanosaeta* dominated the population.

Thermovirga was the most abundant genus in Phase 2 in both AnMBRs. The moderately saline environment likely contributed to the enrichment of *Thermovirga,* as it has a high tolerance towards salinity (Muñoz Sierra et al., 2020).

The second most abundant genus in Phase 2 was *Syntrophorhabdus*, which increased substantially from 6.1 ± 0.9 % to 26.7 ± 1.2 % by the end of the experiment. The increased relative abundance of *Syntrophorhabdus* followed the increasing phenol concentration in the feed. The similar trend between the two reactors suggested that the relatively high abundance of *Syntrophorhabdus* was indicative of the reactors' conversion capacity of phenolics. However, this observation also suggested that nano-magnetite did not have a positive influence on *Syntrophorhabdus*.

Noteworthy, *Mesotoga* species were also found to be more enriched in AnMBR-M relative to AnMBR-C. The contrasting relative abundance of *Mesotoga* between Phase 1 and Phase 2 in AnMBR-M suggests the possible enhancement of the SAO pathway in Phase 2. Fig. 6 shows that the genes *fhs and fdhA* were found to be significantly more abundant in AnMBR-M than in AnMBR-C (for the complete comparison, see Figure S7b, Supplementary materials). However, since only two out of nine genes related to the SAO pathway were more abundant in AnMBR-M, the speculation of SAO pathway stimulation in AnMBR-M in Phase 2 is not as strong as the one in AnMBR-C in Phase 1. Nevertheless, realizing that *Mesotoga* is also known as a short-chain fatty acid degrader (Zhao et al., 2022), the possible role of *Mesotoga* was not limited to solely oxidizing acetate. Additionally, *Mesotoga* was reported to be capable of reducing Fe (III) for methane production (Wen et al., 2025), highlighting their possible role in the higher total Fe concentration in AnMBR-M.

In contrast, *Methanosaeta* exhibited a reduction in relative abundance to 4.1 % in AnMBR C and 6.5 % in AnMBR-M, which was

lower than the values of 20.4 ± 4.8 % found by Garcia Rea et al. (2022). However, despite the overall decline in *Methanosaeta*, *Methanosaeta harundinacea* was notably more enriched in AnMBR-M, with a sixfold increase (Fig. 5b; see the species relative abundance of Phase 1 in Figure S5). *M. harundinacea* was among the few species identified with 100 % confidence (See Table S5, Supplementary materials), supporting the validity of its observed enrichment. Despite belonging to a commonly known acetoclastic genus, this species was reported to have the capacity to reduce CO_2 into methane (Wang et al., 2016; Rotaru et al., 2014).

Interestingly, in contrast with Phase 1, *Pseudomonas* was not enriched in AnMBR-M in Phase 2. The absence of *Pseudomonas* in Phase 2 may have reflected its inability to tolerate the higher phenolic loading rate in Phase 2. This observation also suggested that the enhanced electron transfer mechanisms between the two phases were different. While the results suggest that DIET was successfully stimulated and nano-magnetite may have served as an electron conduit in Phase 1, this may not have been the case in Phase 2, due to the lack of an identified electrogenic electron-donating partner such as *Pseudomonas* or *Geobacter*. Or alternatively, the active electron-donating partner was present in too low abundance or not identified in our analyses. Moreover, the conductivity of biomass in AnMBR-C was higher than AnMBR-M during most of Phase 2 (Figure S6, Supplementary materials). Nevertheless, the higher total Fe concentration in Phase 2 (Fig. 3) may suggest that nano-magnetite enhanced the electron transfer between the syntrophic microorganisms through the dissimilatory Fe reduction-oxidation cycle, as reviewed by Xu et al. (2019). In this reaction cycle, Fe(III) reducing bacteria produce solubilized Fe(II) that subsequently transfers electrons to methanogens to reduce CO_2 to CH_4, while Fe(II) is being re-oxidised to the original Fe(III) mineral. Possibly, such enhanced electron transfer mechanism may have enhanced the degradation rate of VFAs, which in turn enhanced the degradation rate of phenol and p-cresol. Moreover, the Fe-based enhanced electron transfer mechanism might also have facilitated the syntrophic acetate oxidation pathway in Phase 2, where the enriched *Mesotoga* possibly grew in syntrophy with CO_2-reducing methanogens, like the also enriched *M. harundinacea,* as a direct electron acceptor.

4. Conclusions

This study indicated that the supplementation of 20 mmol/L nano-magnetite particles increased the maximum phenolic loading rate of an AnMBR compared to a control reactor without magnetite supplementation. The AnMBR with 20 mmol/L nano-magnetite showed approximately 10 % higher methane yield than the control. Furthermore, magnetite-adapted biomass was less impacted by the toxicity of high phenol concentrations. The adsorption of phenolics onto magnetite was minimal, even at high concentrations, and was calculated to contribute only marginally. While the DIET mechanism between *Pseudomonas* and *Methanolinea* was possibly stimulated in Phase 1, it failed to alleviate the inhibition caused by the excessive 40 mmol/L nano-magnetite supplementation. The dissimilatory iron reduction-oxidation cycle likely enhanced the electron transfer mechanism in AnMBR-M in Phase 2 instead of DIET. Furthermore, *Syntrophorhabdus aromaticivorans* dominated the detected *Syntrophorhabdus* genus in both reactors, comprising over 80 % of its population, regardless of magnetite supplementation. Future research should investigate a broader range of magnetite dosages, the inhibition mechanism of excessive magnetite dosages, and elucidate whether magnetite addition does have a substantial improvement specifically on phenol conversion rates.

CRediT authorship contribution statement

Henri Spanjers: Writing – review & editing, Supervision, Conceptualization. **Jules B. van Lier:** Writing – review & editing, Supervision, Resources, Funding acquisition, Conceptualization. **Daniel Cerqueda-Garcia:** Visualization, Formal analysis, Data curation. **Julian D. Muñoz Sierra:** Writing – review & editing, Visualization, Supervision, Conceptualization. **Eman Rageh:** Methodology, Investigation, Formal analysis. **Beatriz Egerland Bueno:** Investigation. **Rifki Wahyu Kurnianto:** Writing – original draft, Visualization, Methodology, Investigation, Funding acquisition, Formal analysis, Conceptualization. **Mostafa Elshourbagy:** Methodology, Investigation, Formal analysis, Conceptualization.

Declaration of generative AI and AI-assisted technologies in the writing process

During the preparation of this work, the author(s) used QUILLBOT and ChatGPT to paraphrase the English in some parts of the manuscript. After using this tool/service, the author(s) reviewed and edited the content as needed and take(s) full responsibility for the content of the publication.

Declaration of Competing Interest

The authors declare that they have no known competing financial interests or personal relationships that could have appeared to influence the work reported in this paper.

Acknowledgments

We are thankful to the lab technicians Armand Middeldorp and Jasper Krijn for the technical support in the lab. This work was financially supported by Topconsortia voor Kennis en Innovatie (TKI), the Indonesian Education Scholarship (BPI Kemendikbudristek) from the Center for Higher Education Funding (BPPT) Kemendikbudristek Indonesia, and Indonesia Endowment Fund for Education Agency (LPDP).

Appendix A. Supporting information

Supplementary data associated with this article can be found in the online version at doi:10.1016/j.eti.2025.104504.

Data availability

Data will be made available on request.

References

Al-Asheh, S., Bagheri, M., Aidan, A., 2021. Membrane bioreactor for wastewater treatment: a review. Case Stud. Chem. Environ. Eng. 4. https://doi.org/10.1016/j.cscee.2021.100109.

APHA, 1998. *standard methods for the examination of water and wastewater* (20th Editi). American public health association. American Water Works Association and Water Environmental Federation.

Callahan, B.J., McMurdie, P.J., Rosen, M.J., Han, A.W., Johnson, A.J.A., Holmes, S.P., 2016. DADA2: High-resolution sample inference from illumina amplicon data. Nat. Methods 13 (7), 581–583. https://doi.org/10.1038/nmeth.3869.

Castellano-Hinojosa, A., Armato, C., Pozo, C., González-Martínez, A., González-López, J., 2018. New concepts in anaerobic digestion processes: recent advances and biological aspects. Appl. Microbiol. Biotechnol. 102 (12), 5065–5076. https://doi.org/10.1007/s00253-018-9039-9.

Chi, M., Su, X., Sun, X., Xu, Y., Wang, X., Qiu, Y., 2021. Microbial analysis and enrichment of anaerobic phenol and p -cresol degrading consortia with addition of AQDS. Water Sci. Technol. 84 (3), 683–696. https://doi.org/10.2166/wst.2021.264.

Douglas, G.M., Maffei, V.J., Zaneveld, J.R., Yurgel, S.N., Brown, J.R., Taylor, C.M., Huttenhower, C., Langille, M.G.I., 2020. PICRUSt2 for prediction of metagenome functions. Nat. Biotechnol. 38 (6), 685–688. https://doi.org/10.1038/s41587-020-0548-6.

Feng, D., Xia, A., Wu, S., Huang, Y., Zhu, X., Zhu, X., Deepanraj, B., Show, P.-L., Liao, Q., 2022. Magnetite as a means to enhance anaerobic digestion of furfural. J. Clean. Prod. 381, 135139. https://doi.org/10.1016/j.jclepro.2022.135139.

Fernandes, A.D., Macklaim, J.M., Linn, T.G., Reid, G., Gloor, G.B., 2013. ANOVA-Like differential expression (ALDEx) analysis for mixed population RNA-Seq. PLoS One 8 (7), e67019. https://doi.org/10.1371/journal.pone.0067019.

Fernandes, A.D., Reid, J.N., Macklaim, J.M., McMurrough, T.A., Edgell, D.R., Gloor, G.B., 2014. Unifying the analysis of high-throughput sequencing datasets: characterizing RNA-seq, 16S rRNA gene sequencing and selective growth experiments by compositional data analysis. Microbiome 2 (1), 15. https://doi.org/10.1186/2049-2618-2-15.

Freguia, S., Teh, E.H., Boon, N., Leung, K.M., Keller, J., Rabaey, K., 2010. Microbial fuel cells operating on mixed fatty acids. Bioresour. Technol. 101 (4), 1233–1238. https://doi.org/10.1016/j.biortech.2009.09.054.

Gahlot, P., Ahmed, B., Tiwari, S.B., Aryal, N., Khursheed, A., Kazmi, A.A., Tyagi, V.K., 2020. Conductive material engineered direct interspecies electron transfer (DIET) in anaerobic digestion: mechanism and application. Environ. Technol. Innov. 20, 101056. https://doi.org/10.1016/j.eti.2020.101056.

Garcia Rea, V.S., Egerland Bueno, B., Cerqueda-García, D., Muñoz Sierra, J.D., Spanjers, H., van Lier, J.B., 2022. Degradation of p-cresol, resorcinol, and phenol in anaerobic membrane bioreactors under saline conditions. Chem. Eng. J. 430. https://doi.org/10.1016/j.cej.2021.132672.

García Rea, V.S., Muñoz Sierra, J.D., Fonseca Aponte, L.M., Cerqueda-Garcia, D., Quchani, K.M., Spanjers, H., van Lier, J.B., 2020. Enhancing phenol conversion rates in saline anaerobic membrane bioreactor using acetate and butyrate as additional carbon and energy sources. Front. Microbiol 11. https://doi.org/10.3389/fmicb.2020.604173.

García Rea, V.S., Egerland Bueno, B., Muñoz Sierra, J.D., Nair, A., Lopez Prieto, I.J., Cerqueda-García, D., van Lier, J.B., Spanjers, H., 2023. Chemical characterization and anaerobic treatment of bitumen fume condensate using a membrane bioreactor. J. Hazard. Mater. 447, 130709. https://doi.org/10.1016/j.jhazmat.2022.130709.

Guan, Q., Qu, Y., Zhai, Y., Shi, W., Zhao, M., Huang, Z., Ruan, W., 2023. Enhancement of methane production in anaerobic digestion of high salinity organic wastewater: the synergistic effect of nano-magnetite and potassium ions. Chemosphere 318, 137974. https://doi.org/10.1016/j.chemosphere.2023.137974.

Hashemi, B., Horn, S.J., Lamb, J.J., Lien, K.M., 2022. Potential role of sulfide precipitates in direct interspecies electron transfer facilitation during anaerobic digestion of fish silage. Bioresour. Technol. Rep. 20, 101264. https://doi.org/10.1016/j.biteb.2022.101264.

He, C., Lin, W., Zheng, X., Wang, C., Hu, Z., Wang, W., 2019. Synergistic effect of magnetite and zero-valent iron on anaerobic degradation and methanogenesis of phenol. Bioresour. Technol. 291, 121874. https://doi.org/10.1016/j.biortech.2019.121874.

He, J., Wu, F., Zhong, Y., Zhang, P., Zou, X., Pan, X., Zhang, J., 2022. Insight into magnetite effects on anaerobic digestion of waste activated sludge with thermal hydrolysis pretreatment: from reactor performance to metagenomics analysis. J. Water Process Eng. 49, 102963. https://doi.org/10.1016/j.jwpe.2022.102963.

Jung, S., Kim, M., Lee, J., Shin, J., Shin, S.G., Lee, J., 2022. Effect of magnetite supplementation on mesophilic anaerobic digestion of phenol and benzoate: methane production rate and microbial communities. Bioresour. Technol. 350 (February), 126943. https://doi.org/10.1016/j.biortech.2022.126943.

Jung, S., Kim, S.E., Kang, S., Thanh Ngo, T.T., Lee, J., 2024. Effect of magnetite powder dosage on the anaerobic digestion of phenolic wastewater. J. Geol. Soc. Korea 60 (4), 425–432. https://doi.org/10.14770/jgsk.2024.041.

Katoh, K., Standley, D.M., 2013. MAFFT multiple sequence alignment software version 7: improvements in performance and usability. Mol. Biol. Evol. 30 (4), 772–780. https://doi.org/10.1093/molbev/mst010.

Kim, M., Jung, S., Kang, S., Rhie, M.N., Song, M., Shin, J., Shin, S.G., Lee, J., 2024. Magnetite particles accelerate methanogenic degradation of highly concentrated acetic acid in anaerobic digestion process. Environ. Res. https://doi.org/10.1016/j.envres.2024.119132.

Lee, J.-Y., Lee, S.-H., Park, H.-D., 2016. Enrichment of specific electro-active microorganisms and enhancement of methane production by adding granular activated carbon in anaerobic reactors. Bioresour. Technol. 205, 205–212. https://doi.org/10.1016/j.biortech.2016.01.054.

Li, Y., Tabassum, S., Chu, C., Zhang, Z., 2018. Inhibitory effect of high phenol concentration in treating coal gasification wastewater in anaerobic biofilter. J. Environ. Sci. 64, 207–215. https://doi.org/10.1016/j.jes.2017.06.001.

van Lier, J.B., Mahmoud, N., Zeeman, G., 2008. 16 anaerobic wastewater treatment. In Biological Wastewater Treatment: Principles, Modelling and Design. IWA Pub, pp. 401–442.

Lu, T., Su, T., Liang, X., Wei, Y., Zhang, J., He, T., 2022. Dual character of methane production improvement and antibiotic resistance genes reduction by nano-Fe2O3 addition during anaerobic digestion of swine manure. J. Clean. Prod. 376, 134240. https://doi.org/10.1016/j.jclepro.2022.134240.

Ma, W., Li, J., Zhong, D., Ge, X., Li, K., Dai, C., Gao, Y., 2021. New insights into enhanced anaerobic degradation of coal gasification wastewater (CGW) with the assistance of magnetite nanoparticles. Chemosphere 262, 127872. https://doi.org/10.1016/j.chemosphere.2020.127872.

Mazioti, A.A., Koutsokeras, L.E., Constantinides, G., Vyrides, I., 2021. Untapped potential of moving bed biofilm reactors with different biocarrier types for bilge water treatment: a Laboratory-Scale study. Water 13 (13), 1810. https://doi.org/10.3390/w13131810.

McMurdie, P.J., Holmes, S., 2013. Phyloseq: an r package for reproducible interactive analysis and graphics of microbiome census data. PLoS One 8 (4), e61217. https://doi.org/10.1371/journal.pone.0061217.

Mostafa, A., Im, S., Lee, M., Song, Y., Kim, D., 2020. Enhanced anaerobic digestion of phenol via electrical energy input. Chem. Eng. J. 389 (October 2019), 124501. https://doi.org/10.1016/j.cej.2020.124501.

Muñoz Sierra, J.D., Oosterkamp, M.J., Wang, W., Spanjers, H., van Lier, J.B., 2018. Impact of long-term salinity exposure in anaerobic membrane bioreactors treating phenolic wastewater: performance robustness and endured microbial community. Water Res 141, 172–184. https://doi.org/10.1016/j.watres.2018.05.006.

Muñoz Sierra, J.D., García Rea, V.S., Cerqueda-García, D., Spanjers, H., van Lier, J.B., 2020. Anaerobic conversion of saline Phenol-Containing wastewater under thermophilic conditions in a membrane bioreactor. Front. Bioeng. Biotechnol. 8. https://doi.org/10.3389/fbioe.2020.565311.

Nobu, M.K., Narihiro, T., Hideyuki, T., Qiu, Y.L., Sekiguchi, Y., Woyke, T., Goodwin, L., Davenport, K.W., Kamagata, Y., Liu, W.T., 2015. The genome of syntrophorhabdus aromaticivorans strain UI provides new insights for syntrophic aromatic compound metabolism and electron flow. Environ. Microbiol 17 (12), 4861–4872. https://doi.org/10.1111/1462-2920.12444.

Oksanen, J., Blanchet, F.G., Kindt, R., Legendre, P., Minchin, P.R., O'hara, R.B., Simpson, G.L., Solymos, P., Stevens, M.H.H., Wagner, H., Oksanen, M.J., 2013. Package 'vegan'. Community Ecol. Package (2(9), 1–295.

Price, M.N., Dehal, P.S., Arkin, A.P., 2010. FastTree 2 – approximately Maximum-Likelihood trees for large alignments. PLoS One 5 (3), e9490. https://doi.org/10.1371/journal.pone.0009490.

Qiu, Y.-L., Hanada, S., Ohashi, A., Harada, H., Kamagata, Y., Sekiguchi, Y., 2008. Syntrophorhabdus aromaticivorans gen. Nov., sp. Nov., the first cultured anaerobe capable of degrading phenol to acetate in obligate syntrophic associations with a hydrogenotrophic methanogen. Appl. Environ. Microbiol 74 (7), 2051–2058. https://doi.org/10.1128/AEM.02378-07.

Rognes, T., Flouri, T., Nichols, B., Quince, C., Mahé, F., 2016. VSEARCH: a versatile open source tool for metagenomics. PeerJ 4, e2584. https://doi.org/10.7717/peerj.2584.

Rotaru, A.-E., Shrestha, P.M., Liu, F., Shrestha, M., Shrestha, D., Embree, M., Zengler, K., Wardman, C., Nevin, K.P., Lovley, D.R., 2014. A new model for electron flow during anaerobic digestion: direct interspecies electron transfer to methanosaeta for the reduction of carbon dioxide to methane. Energy Environ. Sci. 7 (1), 408–415. https://doi.org/10.1039/C3EE42189A.

Sun, C., Yu, Q., Zhao, Z., Fan, S., Zhang, Y., 2023. Establishment of an electroactive microorganism community in anaerobic digestion with photosynthetic bacteria agents for promoting methane production. ACS Sustain. Chem. Eng. 11 (46), 16521–16529. https://doi.org/10.1021/acssuschemeng.3c04227.

Sun, L., Toyonaga, M., Ohashi, A., Tourlousse, D.M., Matsuura, N., Meng, X.-Y., Tamaki, H., Hanada, S., Cruz, R., Yamaguchi, T., Sekiguchi, Y., 2016. Lentimicrobium saccharophilum gen. Nov., sp. Nov., a strictly anaerobic bacterium representing a new family in the phylum bacteroidetes, and proposal of lentimicrobiaceae fam. Nov. Int. J. Syst. Evol. Microbiol 66 (7), 2635–2642. https://doi.org/10.1099/ijsem.0.001103.

Tang, Y., Li, Y., Zhang, M., Xiong, P., Liu, L., Bao, Y., 2021. Link between characteristics of fe (III) oxides and critical role in enhancing anaerobic methanogenic degradation of complex organic compounds. Environ. Res. 194 (October 2020), 110498. https://doi.org/10.1016/j.envres.2020.110498.

Wang, L.-Y., Nevin, K.P., Woodard, T.L., Mu, B.-Z., Lovley, D.R., 2016. Expanding the diet for DIET: electron donors supporting direct interspecies electron transfer (DIET) in defined Co-Cultures. Front. Microbiol 7. https://doi.org/10.3389/fmicb.2016.00236.

Wang, Z., Wang, T., Si, B., Watson, J., Zhang, Y., 2021. Accelerating anaerobic digestion for methane production: potential role of direct interspecies electron transfer. In: In Renewable and Sustainable Energy Reviews, 145. Elsevier Ltd. https://doi.org/10.1016/j.rser.2021.111069.

Wen, H.-Q., Chen, G.-L., Li, Y.-S., Tian, T., Pan, Y., Yu, H.-Q., 2025. An inconvenient impact: unveiling the overlooked differences in crystalline forms of iron (hydro) oxides on anaerobic digestion. Water Res. X 26, 100286. https://doi.org/10.1016/j.wroa.2024.100286.

Xu, H., Chang, J., Wang, H., Liu, Y., Zhang, X., Liang, P., Huang, X., 2019. Enhancing direct interspecies electron transfer in syntrophic-methanogenic associations with (semi)conductive iron oxides: effects and mechanisms. Sci. Total Environ. 695. https://doi.org/10.1016/j.scitotenv.2019.133876.

Yan, W., Sun, F., Liu, J., Zhou, Y., 2018. Enhanced anaerobic phenol degradation by conductive materials via EPS and microbial community alteration. Chem. Eng. J. 352 (April), 1–9. https://doi.org/10.1016/j.cej.2018.06.187.

Yang, J., Liu, K., Yi, W., Si, B., Tian, C., Yang, G., 2024. Effects of biochar, granular activated carbon, and magnetite on the electron transfer of microbials during the anaerobic digestion process: insights into nitrogen heterocyclic compounds degradation. Fuel 358, 130079. https://doi.org/10.1016/j.fuel.2023.130079.

Yilmaz, P., Yarza, P., Rapp, J.Z., Glöckner, F.O., 2016. Expanding the world of marine bacterial and archaeal clades. Front. Microbiol 6. https://doi.org/10.3389/fmicb.2015.01524.

Zhao, Y., Li, Q., Cui, Q., Ni, S.-Q., 2022. Nitrogen recovery through fermentative dissimilatory nitrate reduction to ammonium (DNRA): carbon source comparison and metabolic pathway. Chem. Eng. J. 441, 135938. https://doi.org/10.1016/j.cej.2022.135938.

Zhao, Z., Zhang, Y., Yu, Q., Dang, Y., Li, Y., Quan, X., 2016. Communities stimulated with ethanol to perform direct interspecies electron transfer for syntrophic metabolism of propionate and butyrate. Water Res 102, 475–484. https://doi.org/10.1016/j.watres.2016.07.005.